A local-global scheme for tracking crack path in three-dimensional solids

O.L. Manzoli[*], G.K.S. Claro, E.A. Rodrigues and J.A. Lopes Jr.

Department of Civil Engineering, Univ Estadual Paulista - UNESP,
Av. Luiz Edmundo C. Coube,' 14-01, 17033-360, Bauru, SP, Brazil

Abstract. This paper aims to contribute to the three-dimensional generalization of numerical prediction of crack propagation through the formulation of finite elements with embedded discontinuities. The analysis of crack propagation in two-dimensional problems yields lines of discontinuity that can be tracked in a relatively simple way through the sequential construction of straight line segments oriented according to the direction of failure within each finite element in the solid. In three-dimensional analysis, the construction of the discontinuity path is more complex because it requires the creation of plane surfaces within each element, which must be continuous between the elements. In the method proposed by Chaves (2003) the crack is determined by solving a problem analogous to the heat conduction problem, established from local failure orientations, based on the stress state of the mechanical problem. To minimize the computational effort, in this paper a new strategy is proposed whereby the analysis for tracking the discontinuity path is restricted to the domain formed by some elements near the crack surface that develops along the loading process. The proposed methodology is validated by performing three-dimensional analyses of basic problems of experimental fractures and comparing their results with those reported in the literature.

Keywords: embedded crack element; fracture; three-dimensional analysis; crack path

1. Introduction

Progress has been made in the search for methodologies that are able to describe the path of discontinuities in quasi-brittle materials without the need to adapt the finite element grid as the crack advances. The existing techniques include Enriched Finite Element Methods, which can be divided into two groups (Oliver *et al.* 2006). One of these is Element Enrichment, which comprises finite elements with embedded discontinuities based on enrichment of the displacement field of each element to represent the effects of the discontinuity that passes through it, known as E-FEM and originally described by Ortiz *et al.* (1987). The second group is that of Nodal Enrichment, comprising generalized or extended finite elements (X-FEM), which is based on the enrichment of the interpolation functions associated with existing nodes and was first proposed by Melenk and Babuska (1996).

For both types of enrichment to represent the effect of the crack inside the finite element, it is

---

*Corresponding author, Professor, E-mail: khkwan@hku.hk

necessary to use algorithms that track its path. Jäger *et al*. (2008) classify these algorithms into *fixed crack tracking*, *local crack tracking*, *non-local crack tracking*, and *global crack tracking* schemes.

The simplest of these algorithms is the fixed crack path tracking scheme, for which the crack path must be known a priori. In this case, the path is no longer an unknown component in the problem and the elements traversed by the potential crack surface, as well as its position inside each of these elements, are previously defined. Therefore, during the loading process, the elements of this set may fail, i.e., their discontinuity surface may be activated as the stresses approach the failure criterion. Since the potential failure surface defined *a priori* is continuous between finite elements, the final active surface will also be continuous. The analysis in this case will undergo interference only from the order in which the elements crossed by the potential failure surface are activated as a function of the load level, since the path remains unchanged. According to Jäger *et al*. (2008), from the computational standpoint, this algorithm is particularly robust and stable.

The local crack tracking scheme can be interpreted as the generalization to three-dimensional fractures of the algorithm presented by Manzoli (1998). According to this technique, the crack essentially extends from points of discontinuity in elements adjacent to the element with the active crack and follows in the normal direction of the maximum principal stress. Since this concept could, eventually, yield irregular and discontinuous surfaces, Areias and Belytschko (2001) suggested adjusting the normal failure plane based on the intersection points of the crack of the neighboring element with the element containing the active failure.

Another existing technique is the non-local crack tracking scheme, which calculates the mean direction of the failure plane along a neighborhood. Gasser and Holzapfel (2006) affirm that, on average, the discontinuous surface thus generated is regular. In other words, the vector normal to the crack plane, which is calculated from the direction of the maximum principal stress, is not only adapted to the points of the neighboring elements. Instead, the method also takes into account the information of all the crack points inside a sphere around the center of the analyzed element. Although this is a theoretically elegant methodology, it is very inconvenient to include it in existing finite element codes.

Lastly, there is the global crack tracking scheme, which presents a specific finite element solution for a crack problem, characterized by an additional unknown scalar value, which defines one or multiple crack surfaces as isosurfaces. The purpose of this proposed algorithm by Oliver and Huespe (2004) is to find a scalar field $\theta(x, t)$ so that isovalue surfaces become potential discontinuity surfaces. Therefore, the vector field given by the vectors normal to isovalue surfaces, $\theta, \nabla\theta$, should coincide with the vector fields normal to the potential failure surface, which are established by the failure criterion calculated from the stresses (or strains) of the mechanical problem.

The global crack path tracking methodology involves high computational effort, since it requires solving an additional global system of equations besides the one pertaining to the mechanical problem. Nevertheless, the methodology is easy to include in existing finite element programs, and is more flexible and stable than the other crack path tracking strategies.

In this work, the element enrichment method was adopted as a tool to predict the behavior of the crack inside the finite element. An extension for three-dimensional problems of the embedded discontinuity finite element proposed by Manzoli and Shing (2006) and Manzoli (2008) is used.
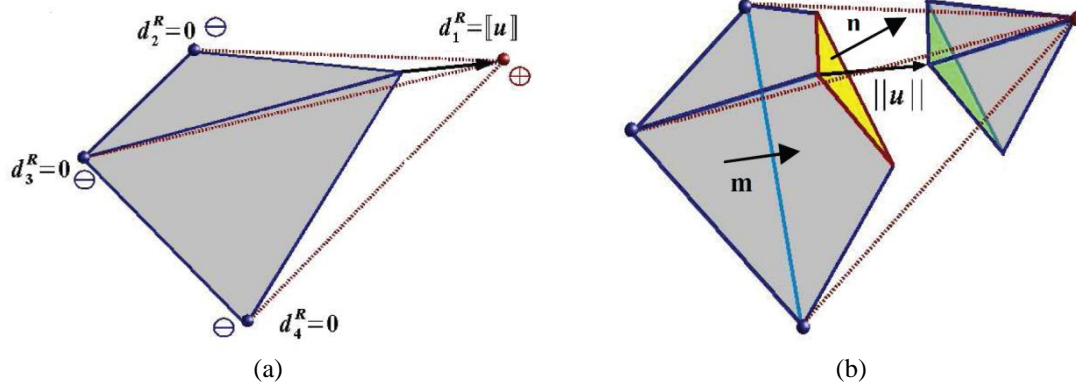
Fig. 1 (a) Three-dimensional element, (b) relative displacements due to the discontinuity, with one isolated node

2. Finite elements with embedded discontinuities

Let the four-node tetrahedral element of the three-dimensional domain Ω_e containing a discontinuous surface, S, be such that it divides the element into two parts, isolating one or two nodes from the others. Let $\boldsymbol{n} = \{n_x\ n_y\ n_z\}^T$ be the unitary vector normal to the surface, S, and $\boldsymbol{m} = \{m_x\ m_y\ m_z\}^T$ the unitary vector corresponding to the gradient of the sum of the shape functions of the isolated nodes (one or two, depending on the position of the crack in the element). Note that if there is only one isolated node, $\boldsymbol{m}$ corresponds to a vector normal to the opposite side of the single node, as shown in Fig. 1(b).

The discontinuity causes a relative displacement of the isolated node in relation to the others, as illustrated in Fig. 1 and expressed by

$$\boldsymbol{d}_1^R = [\![\boldsymbol{u}]\!] \tag{1a}$$

$$\boldsymbol{d}_2^R = \boldsymbol{0} \tag{1b}$$

$$\boldsymbol{d}_3^R = \boldsymbol{0} \tag{1c}$$

$$\boldsymbol{d}_4^R = \boldsymbol{0} \tag{1d}$$

where the vector $\boldsymbol{d}_i^R$ ($i = 1,2,3\ and\ 4$) represents the components of the displacements of each node produced by the discontinuity, and $[\![\boldsymbol{u}]\!]$ is the vector of the components of the relative node displacements on the discontinuous surface, as shown in Fig. 1.

The node displacements produced by the discontinuity, $\boldsymbol{d}_i^R$, are associated to the rigid body motion between the two portions of the element separated by the discontinuity. Hence, upon determining the strains, $\boldsymbol{\varepsilon} = \{\varepsilon_x\ \varepsilon_y\ \gamma_{xy}\ \varepsilon_z\ \gamma_{yz}\ \gamma_{xz}\}^T$, from the node displacements of the element, $\boldsymbol{d}_i$, the component of the node displacements associated with the discontinuity, $\boldsymbol{d}_i^R$ must be subtracted, i.e.

$$\boldsymbol{\varepsilon} = \sum_{i=1}^{4} \boldsymbol{B}_i\left(\boldsymbol{d}_i - \boldsymbol{d}_i^R\right) \tag{2}$$

$$\boldsymbol{\varepsilon} = \sum_{i=1}^{4} \boldsymbol{B}_i d_i - \boldsymbol{B}_1 [\![\boldsymbol{u}]\!] \tag{3}$$

$$\boldsymbol{\varepsilon} = \boldsymbol{B}\boldsymbol{d} - \boldsymbol{\varepsilon}^R \tag{4}$$

where the $\boldsymbol{B}$ matrix groups together the conventional $\boldsymbol{B}_i$ matrices (strain-displacement matrices) of the Finite Element Method (FEM), vector $\boldsymbol{d}$ groups the vectors of node displacements of all the element nodes, and $\boldsymbol{d}_i$, and $\boldsymbol{\varepsilon}^R = \boldsymbol{B}_1 [\![\boldsymbol{u}]\!]$ correspond to the part of the strain associated with the rigid body displacement produced by the discontinuity

$$
\begin{Bmatrix} \varepsilon_x^R \\ \varepsilon_y^R \\ \gamma_{xy}^R \\ \varepsilon_z^R \\ \gamma_{yz}^R \\ \gamma_{xz}^R \end{Bmatrix} =
\begin{bmatrix}
\frac{\partial N_1}{\partial x} & 0 & 0 \\
0 & \frac{\partial N_1}{\partial y} & 0 \\
\frac{\partial N_1}{\partial y} & \frac{\partial N_1}{\partial x} & \frac{\partial N_1}{\partial z} \\
0 & 0 & \frac{\partial N_1}{\partial z} \\
0 & \frac{\partial N_1}{\partial z} & \frac{\partial N_1}{\partial y} \\
\frac{\partial N_1}{\partial z} & 0 & \frac{\partial N_1}{\partial x}
\end{bmatrix}
\begin{Bmatrix} [\![u]\!]_x \\ [\![u]\!]_y \\ [\![u]\!]_z \end{Bmatrix} =
\frac{1}{l_e}
\begin{bmatrix}
m_x & 0 & 0 \\
0 & m_y & 0 \\
m_y & m_x & 0 \\
0 & 0 & m_z \\
0 & m_z & m_y \\
m_z & 0 & m_x
\end{bmatrix}
\begin{Bmatrix} [\![u]\!]_x \\ [\![u]\!]_y \\ [\![u]\!]_z \end{Bmatrix} \tag{5}
$$

where N_1 is a conventional shape function of the FEM associated with the isolated node.

In Eq. (5), l_e is the "characteristic length" of the element, which is evaluated as the inverse of the norm of the gradient vector of the sum of the shape functions of the isolated nodes (one or two isolated nodes, depending on the crack position in the interior of the element). Note that in the case illustrated here of only one isolated node, l_e corresponds to the distance between the single node and the opposite side. Therefore, Eq. (5) considers that

$$\left\{ \frac{m_x}{l_e}, \frac{m_y}{l_e}, \frac{m_z}{l_e} \right\} = \left\{ \frac{\partial N_1}{\partial x}, \frac{\partial N_1}{\partial y}, \frac{\partial N_1}{\partial z} \right\} \tag{6}$$

Considering a linear elastic behavior in the continuous part of the element, the stresses $\boldsymbol{\sigma} = \{\sigma_x \quad \sigma_y \quad \gamma_{xy} \quad \sigma_z \quad \gamma_{yz} \quad \gamma_{xz}\}$ can be obtained by

$$\boldsymbol{\sigma} = \boldsymbol{E}\boldsymbol{\varepsilon} \tag{7}$$

$$\boldsymbol{\sigma} = \boldsymbol{E}(\boldsymbol{B}\boldsymbol{d} - \boldsymbol{\varepsilon}^R) \tag{8}$$

where $\boldsymbol{E}$ is the linear elastic constitutive matrix. As can be seen in Eq. (8), the $\boldsymbol{\varepsilon}^R$ strains play the role of inelastic strains that are compatible with the relative displacement of the single node originating from the discontinuity.

Given that the stresses in the element are constant, the vector of internal forces of the element can be expressed by

$$\boldsymbol{f}_{int} = \int \boldsymbol{B}^T \boldsymbol{\sigma} \, d\Omega_e \tag{9}$$

$$\boldsymbol{f}_{int} = \boldsymbol{B}^T \boldsymbol{\sigma} V_e \tag{10}$$

where V_e is the volume of the finite element.

The formulation of the finite element with embedded discontinuity is completed by introducing the discrete interface constitutive law, $\boldsymbol{t}([\![u]\!])$, which establishes the relationship between the

components of the discontinuity and the surface forces, together with the condition of continuity between the surface forces of the continuous part and the interface

$$t(\llbracket u \rrbracket) - N^T \sigma = 0 \tag{11}$$

From Eqs. (5) and (8), Eqs. (10) and (11) can be rewritten as

$$f_{int} = B^T E \left(Bd - \frac{M}{l_e} \llbracket u \rrbracket \right) V_e \tag{12}$$

$$t(\llbracket u \rrbracket) - N^T E \left(Bd - \frac{M}{l_e} \llbracket u \rrbracket \right) = 0 \tag{13}$$

where

$$N^T = \begin{bmatrix} n_x & 0 & n_y & 0 & 0 & n_z \\ 0 & n_y & n_x & 0 & n_z & 0 \\ 0 & 0 & 0 & n_z & n_y & n_x \end{bmatrix} \tag{14}$$

$$M^T = l_e B_1^T = \begin{bmatrix} m_x & 0 & m_y & 0 & 0 & m_z \\ 0 & m_y & m_x & 0 & m_z & 0 \\ 0 & 0 & 0 & m_z & m_y & m_x \end{bmatrix} \tag{15}$$

In an incremental and iterative procedure, Eq. (13) is used to calculate the displacement jumps in the element, $\llbracket u \rrbracket$, for a given nodal displacement vector, d. Eq. (12) is then used to calculate the internal forces of the element.

Note that this formulation requires the use of an algorithm that can indicate which nodes will be isolated by the discontinuity, and also the direction of the discontinuity surface, i.e., the position of the discontinuity surface inside the element. One of the existing techniques for this purpose is the global crack path tracking algorithm, which is the basis of this work.

The discrete constitutive model assumed in this paper is based on the damage theory and can be described by the following set of equations

$$t = (1 - d)\bar{t}; \bar{t} = C \llbracket u \rrbracket \quad \text{(constitutive relation)} \tag{16}$$

$$f(\bar{t}_n, r) = \bar{t}_n - r \leq 0 \quad \text{(damage criterion)} \tag{17}$$

$$r = max_{s \in [0,t]}[f_t, t_n(s)] \quad \text{(strain-like internal variable evolution)} \tag{18}$$

$$d = 1 - \frac{f_t}{r} e^{A(1 - r/f_t)}; A = k \frac{f_t^2}{EG_f} \quad \text{(damage evolution)} \tag{19}$$

where d is the damage variable, $\bar{t}$ is the elastic effective traction vector, $\bar{t}_n$ is the traction component normal to the crack surface, r is the strain-like internal variable that assumes the maximum value between $\bar{t}_n$ and the tensile strength, f_t, during the analysis (see equation (18)), G_f is the fracture energy and C is the elastic constitutive matrix, which, according to the local system of coordinates (n,s,t) shown in Fig. 2, is given by

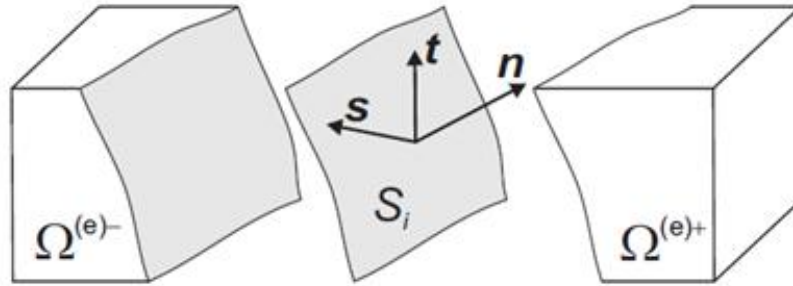$$C = \frac{1}{k} \begin{bmatrix} E & 0 & 0 \\ 0 & G & 0 \\ 0 & 0 & G \end{bmatrix} \tag{20}$$

Fig. 2 Finite element with discontinuity surface S_1 normal to *n* (Blanco 2007)

where *E* is the Young's modulus, *G* is the shear modulus and *k* is a small parameter used to penalize the relative displacement during the elastic regime. It has been assumed $k = 0.1$ mm for the examples presented in this paper.

3. Global crack-tracking algorithm

This section describes the global algorithm (Chaves 2003, Oliver and Huespe 2004), as well as the formulation involved in the algorithm corresponding to the solution of an analogous heat conduction problem and corresponding finite element approximation.

3.1 Steps to solve the global crack-tracking algorithm

The algorithm requires information about the vector field that determines the normal direction of crack propagation in the entire domain under analysis. This can be found from the stress or strain fields obtained from the solution of the mechanical problem.

The algorithm solves a problem analogous to a heat conduction problem, identifying a scalar value that describes the path of the surface crack. Therefore, before beginning the analysis, it is necessary to prescribe scalar values in at least two different nodes of the finite element mesh.

Furthermore, at the beginning of each loading step, the status of the failure surface within the finite element must be updated, indicating whether or not there is active failure, i.e., if the failure criterion was reached or not. When the stress state of the element reaches the failure criterion (the failure becomes active), the orientation of the corresponding failure plane is not changed in the rest of the analysis. This means that the scalar value of the nodes of the element that reaches the failure criterion will remain fixed until the end of the analysis.

Oliver and Huespe (2004) present the failure surface construction process in steps, which can be described as follows

Draw the isosurfaces
For each scalar value found by solving the equivalent thermal problem based on the field vector of normal propagation directions, one has isovalue surfaces.
Identify the active failure surface and its corresponding value
At least one of the isosurfaces found will be the potential failure surface. The active failure

surface is given based on the failure criterion and the scalar value of reference. The reference value is determined by averaging the nodal values of the first element to reach the failure criterion. The active crack surface in the first element that met the failure criterion passes through the centroid of the element and will be called the root element.

Determine the position of the crack in the elements neighboring the root element

The position of the discontinuity is determined based on the scalar value of the surface built in the root element (reference value). To determine the location of the discontinuity inside elements, a linear interpolation of the scalar value of each node of the element is performed. Thus, one determines the points belonging to the edges of the element that present the reference value.

Fix the direction of crack propagation

Once the element has met the failure criterion, the scalar values of the nodes in this element will remain fixed until the end of the numerical analysis.

The process of constructing the discontinuity inside the finite elements takes place successively, as described in steps three and four, until the end of the analysis.

3.2 Formulation of the equivalent heat conduction problem

Let $\boldsymbol{n}(x,t) = \begin{Bmatrix} n_x \\ n_y \\ n_z \end{Bmatrix}$ be a vector normal to the discontinuity surface. For each point x of domain Ω, it is possible to define two vectors $\boldsymbol{s}$ and $\boldsymbol{t}$ orthogonal to $\boldsymbol{n}$ and to each other, i.e.

$$\boldsymbol{s} \cdot \boldsymbol{n} = \boldsymbol{t} \cdot \boldsymbol{n} = 0 \tag{21}$$

Starting from the $\boldsymbol{s}$ and $\boldsymbol{t}$ vectors, it is possible to build a tangent plane to the direction of crack propagation, as shown in Fig. 2.

It is also possible to determine an anisotropic conductivity tensor from the $\boldsymbol{s}$ and $\boldsymbol{t}$ vectors

$$\boldsymbol{K}\big(\boldsymbol{s}(x), \boldsymbol{t}(x)\big) = \boldsymbol{s} \otimes \boldsymbol{s} + \boldsymbol{t} \otimes \boldsymbol{t} \tag{22a}$$

$$\boldsymbol{K}\big(\boldsymbol{s}(x), \boldsymbol{t}(x)\big) = \begin{bmatrix} s_1^2 + t_1^2 & s_1 s_2 + t_1 t_2 & s_1 s_3 + t_1 t_3 \\ s_2 s_1 + t_2 t_1 & s_2^2 + t_2^2 & s_2 s_3 + t_2 t_3 \\ s_3 s_1 + t_3 t_1 & s_3 s_2 + t_3 t_2 & s_3^2 + t_3^2 \end{bmatrix} \tag{22b}$$

so that a flow vector can be defined as

$$\boldsymbol{q}(x,t) = -\boldsymbol{K} \cdot \nabla\theta \tag{23}$$

The family of surfaces given by the orthogonal vectors can be described by a scalar function $\theta(x)$, as follows

$$S_i = \{\boldsymbol{x} \in \Omega;\ \theta(x) = \theta_i\}, \text{ with } \theta_i \in R \tag{24}$$

At each point in the domain, these surfaces are tangent to vectors $\boldsymbol{s}$ and $\boldsymbol{t}$, and these vectors are normal to vector $\boldsymbol{n}$. Thus, the vector field that points in the direction normal to the discontinuity surface should be equal to the gradient of $\theta(x)$, i.e. $\nabla\theta = \boldsymbol{n}$. Hence
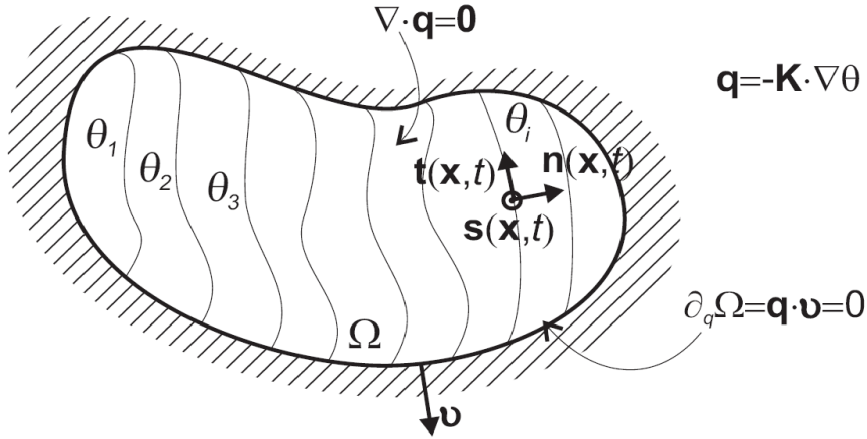
Fig. 3 Problem of thermal boundary values (Blanco 2007)

$$\boldsymbol{s} \cdot \nabla\theta = \nabla\theta \cdot \boldsymbol{s} = 0 \text{ in } \Omega \tag{25a}$$

$$\boldsymbol{t} \cdot \nabla\theta = \nabla\theta \cdot \boldsymbol{t} = 0 \text{ in } \Omega \tag{25b}$$

The solution to Eqs. (25a) and (25b) is also the solution to the heat conduction problem shown in Fig. 3, whose objective is to find $\theta(x)$ that satisfies the following conditions

$$\boldsymbol{\nabla} \cdot \boldsymbol{q} = 0, \text{ in } \Omega \tag{26}$$

$$\boldsymbol{q} = -\boldsymbol{K} \cdot \boldsymbol{\nabla}\theta, \text{ in } \Omega \tag{27}$$

$$\boldsymbol{q} \cdot \boldsymbol{\nu} = 0, \text{ in } \partial_q\Omega \tag{28}$$

$$\theta = \theta^*, \text{ in } \partial_\theta\Omega \tag{29}$$

where $\boldsymbol{\nu}$ is a vector normal to the boundary of the solid, and $\partial\Omega = \partial_\theta\Omega \cup \partial_q\Omega$ and θ^* represents the prescribed values of θ at the boundary.

3.3 Finite element approximation

The heat conduction problem can be solved from its weak form, which is obtained by the weighted residual method. Thus, the weak form of Eq. (26), (27) and (28) can be rewritten as:

$$\int_\Omega (\boldsymbol{\nabla}W)^{\mathrm{T}} \cdot \boldsymbol{K} \cdot \boldsymbol{\nabla}\theta d\Omega = \int_{\Gamma=\Gamma_\theta+\Gamma_q} W \cdot \boldsymbol{q}^T \cdot \boldsymbol{\nu} \, d\Gamma \tag{30}$$

where W are weighting functions.

From the boundary condition in Eq. (28), Eq. (30) is now given by

$$\int_\Omega (\boldsymbol{\nabla}W)^{\mathrm{T}} \cdot \boldsymbol{K} \cdot \boldsymbol{\nabla}\theta d\Omega = 0 \tag{31}$$

Given a domain Ω discretized in n_e finite elements and n_n nodes for each finite element, function $\theta(x)$ can be approximated by shape functions for each finite element

$$\theta^e(x) = \boldsymbol{N}^e \cdot \theta^e \qquad \theta|_{\partial_\theta \Omega} = \theta^* \tag{32}$$

where $\boldsymbol{\theta}^e$ represents the vector of the nodal values of θ for a finite element and $\boldsymbol{N}^e$ are the element's conventional shape functions.

Applying the Galerkin Method and substituting Eq. (32) in Eq. (31), one has

$$\sum \int_{\Omega_e} (\boldsymbol{\nabla N}^e)^{\mathrm{T}} \cdot \boldsymbol{K} \cdot \boldsymbol{\nabla N}^e \cdot \theta^e \, d\Omega = 0 \tag{33}$$

where $\sum$ is a standard assembly operator of finite elements (Hughes 2000).

Eq. (33) can be written compactly as follows

$$\mathbb{K} \cdot \boldsymbol{\theta} = \boldsymbol{0} \tag{34}$$

where $\boldsymbol{\theta}$ is the global vector of nodal scalar values and $\mathbb{K}$ represents the global stiffness matrix composed of the elementary stiffness matrices, given by

$$\mathbb{K}^e = \int_{\Omega_e} (\boldsymbol{\nabla N}^e)^{\mathrm{T}} \cdot \boldsymbol{K} \cdot \boldsymbol{\nabla N}^e \, d\Omega \tag{35}$$

such that

$$\mathbb{K} = \sum_{e=1}^{n_e} \mathbb{K}^e \tag{36}$$

and

$$\boldsymbol{\theta} = \sum_{1}^{n_n} \boldsymbol{\theta}^e \tag{37}$$

Finding the scalar value of all the nodes consists of solving the following linear system

$$\begin{cases} \mathbb{K} \cdot \boldsymbol{\theta} = \boldsymbol{0} \\ \theta|_{\partial_\theta \Omega} = \theta^* \end{cases} \tag{38}$$

3.4 Delineation of potential crack surfaces

As soon as the discontinuity is detected in a finite element (root element), the mean value of θ in the element is determined by the arithmetic mean of the nodal values, as follows

$$\theta_i = \frac{1}{n} \sum_{1}^{n} \theta \tag{39}$$

where *n* corresponds to the number of nodes of the element.

The mean value, θ_i, of the root element will be used to determine the position of the discontinuity in the neighboring finite elements and will, thereafter, be called the reference value. The reference value corresponds to a potential failure surface, S_i, which can be built integrally in the domain.

Once the nodal scalar values and reference value have been found, the position of the
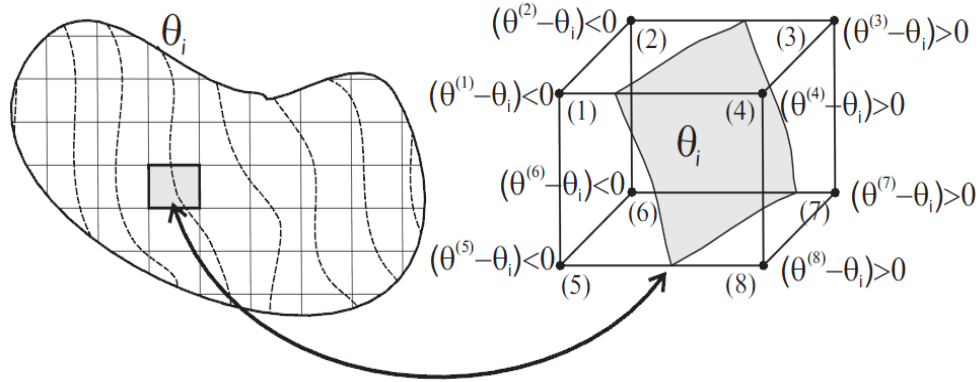
Fig. 4 Construction of potential failure surfaces based on the mean value of θ_i (Blanco 2007)
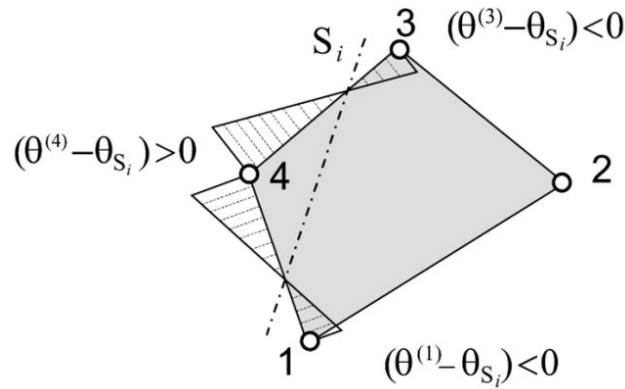

Fig. 5 Linear interpolation for a quadrilateral 2D finite element (Blanco 2007)

discontinuity surface, S_i, in a given finite element can be found by means of the difference between the nodal value and the reference value $(\theta - \theta_i)$, enabling the identification of the vertices for which negative and positive values were obtained, i.e., determine the edges that involve a change in signal, as illustrated in Fig. 4.

Lastly, to identify the position of the discontinuity surface at the edges of the elements possessing nodes (vertices) that involved a change in signal, a linear interpolation is performed as illustrated in Fig. 5.

4. Local-global tracking algorithm

This work proposes an algorithm to identify the crack path based on the global crack tracking algorithm proposed by Oliver and Huespe (2004), introducing a modification that can reduce the computational effort involved. The basic concept consists of building the system of additional equations (corresponding to the crack path problem) only for the elements located in the region close to the failure surface instead of taking up the entire domain of the mechanical problem, as is the case of the global crack tracking algorithm.

4.1 Proposed crack tracking algorithm

Like the global algorithm, one of the initial conditions of the proposed algorithm is that the vector field n of directions normal to the discontinuity surface be known.

Another required initial condition is the establishment of scalar values in two different nodes of the finite element mesh. In the proposed methodology, these values are imposed on two nodes of the first finite element that reaches the failure criterion (root element). The values of the two nodes are established as -1.0 and 1.0 to ensure a reference value of zero.

At the beginning of each loading step, the status of the discontinuity surface inside the element is updated, indicating if the failure criterion was or was not reached. If the failure criterion in an element is reached, the position of the crack in this element is determined by linear interpolation.

The proposed crack tracking algorithm can be described by the following steps:

Topology of the problem
This consists of storing the data of the finite element mesh so that the algorithm can more rapidly identify the elements neighboring the sides of the elements that reach the failure criterion. This is done for all elements only one time before the analysis, in a pre-process stage.

Construction of the potential failure surface in the first element with active failure
Because the values -1.0 and 1.0 were established for two of the four nodes of the first tetrahedral finite element to reach active failure, the algorithm finds the scalar value only of the other two nodes. It then finds the failure surface that corresponds to the null scalar value, which is the reference value for the next steps. As soon as the failure criterion in this element is reached, the nodal scalar values of this element will be fixed until the end of the analysis, and their values will become input data for the next loading step.

Identification of the crack path in the neighboring elements
In the loading step following the consolidation of the failure surface in the first finite element (root element), the proposed algorithm identifies the elements that have a vertex or edge coincident with the root element, which then become part of the domain of analysis, thus becoming candidate elements for failure. The identification of these neighboring elements is easily and rapidly done by means of the information about the mesh topology generated in the step 1. These elements and the involved nodes are then locally numbered and the local connectivity information is updated accordingly in order to assemble the stiffness matrix of the local problem.

The scalar nodal value of all these elements is then found and the nodes that are isolated by the discontinuity surface are identified. Like in the preceding step, upon meeting the failure criterion, the scalar value of the nodes of the new crack element is fixed for all the subsequent loading steps, and their neighboring elements are included in the domain of analysis.

Construction of the failure surface of the solid
Step three is repeated until the end of the analysis.

It should be noted that in each loading step, the mechanical problem indicates for the equivalent heat conduction problem whether any element has met the failure criterion. The equivalent heat conduction problem, in turn, indicates which nodes are isolated by the discontinuity, so that the element is treated by the mechanical problem as a finite element with embedded discontinuity.
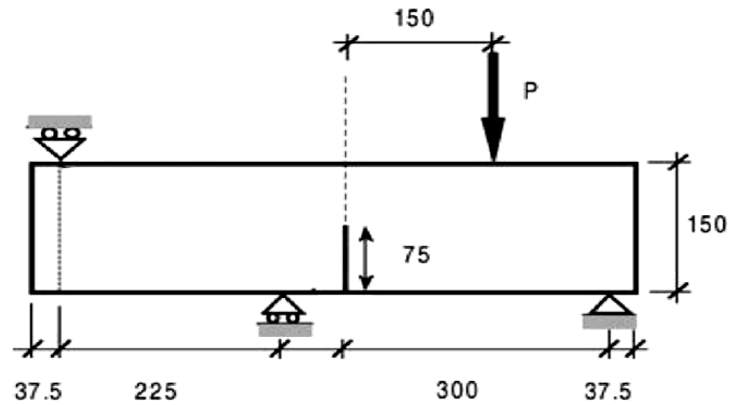
Fig. 6 Geometry (in mm) and boundary conditions (Gálvez *et al.* 1998)
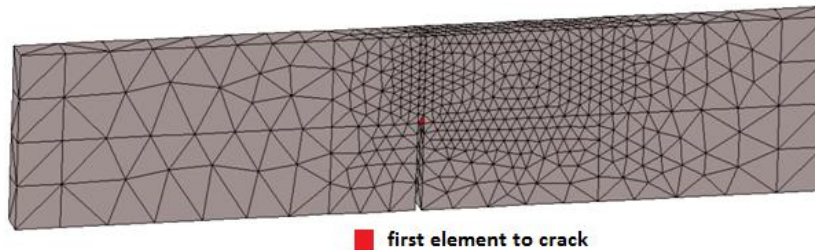

Fig. 7 Original finite element grid, with the first candidate element to crack
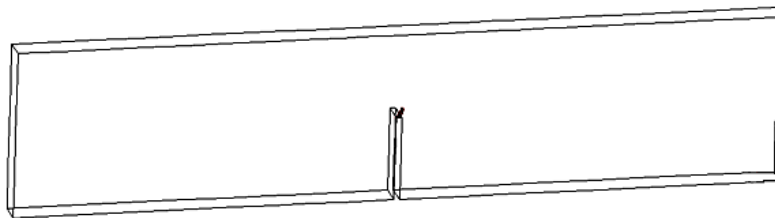

Fig. 8 Result of the first loading steps, which triggered the onset of the crack surface

5. Numerical analysis

The material used in the simulations was concrete, whose properties are presented together with the geometry of each analyzed case. Non-structured mesh of tetrahedral finite element (with four nodes) was used. A limit over the maximum principal stress was adopted as the failure criterion and a tensile damage model was used as a cohesive constitutive model in the discontinuity interface.

5.1 Notched beam subjected to four-point loading

To validate the proposed algorithm, the first analysis corresponds to the test performed by Gálvez, Elices *et al.* (1998). This analysis involves a 50-mm-thick notched beam subjected to four-point bending loads, whose geometry and boundary conditions are illustrated in Fig. 6 while its

experimental parameters are: $G_F = 69$ N/m, $f_t = 3.0$ MPa, $E = 38$ GPa and $v = 0.2$, where G_F is the fracture energy, f_t is the tensile strength, E is the Young's modulus and v is the Poisson's ratio.

Fig. 7 shows the finite element mesh used in the analysis, composed of 4534 elements and 1262 nodes. The red element is the first element to fail. The beam thickness used here was half of its measure (25 mm), due to the symmetry of the problem.

The first element reaches the failure criterion (the failure was activated) after the first loading steps. The corresponding crack surface inside the element is illustrated in Fig. 8. For the subsequent loading steps the crack propagation path is consolidated, i.e., the scalar values of the nodes of the cracked element are fixed until the end of the simulation.

In the loading steps following the consolidation of the crack in the root element, only its neighboring elements are part of the analysis, i.e., the candidate elements for failure. As soon as one of the candidate elements reaches the failure criterion, its direction of propagation is also fixed and the new domain of analysis is updated, being composed of the finite elements neighboring the second element that met the failure criterion.

The crack surface is thus built along successive loading steps. Fig. 9 reinforces the fact that the discontinuity built in the analysis really crosses the finite elements, without adaptation of the finite element mesh.

Once the position of the crack is defined, the embedded discontinuity formulation is able to describe the effect of the crack inside the elements. Fig. 10 illustrates the deformed configuration in an advanced stage of loading.

Since the algorithm does not analyze the entire domain of the model, after all the loading steps, the region involved in the solution of the problem is restricted solely to the green and blue region depicted in Fig. 11. The blue elements represent elements with active cracks while the green elements represent the neighbor elements defining domain of the tracking analysis. In this case the benefits of the proposed scheme are evident. At the beginning of the analysis the domain of the tracking problem is composed by the root and its neighboring elements (14 elements) and at the end of the analysis the domain is composed only by 712 elements (245 nodes). The global tracking algorithm would use the complete mesh composed by 4534 elements and 1262 nodes during the entire analysis, involving 1262 degrees of freedom (one per node) instead of a maximum of 245 involved in the proposed scheme.
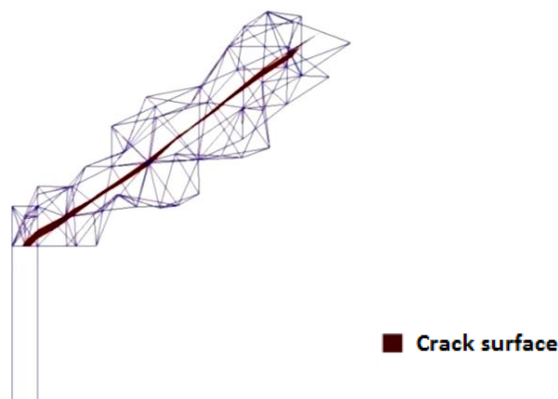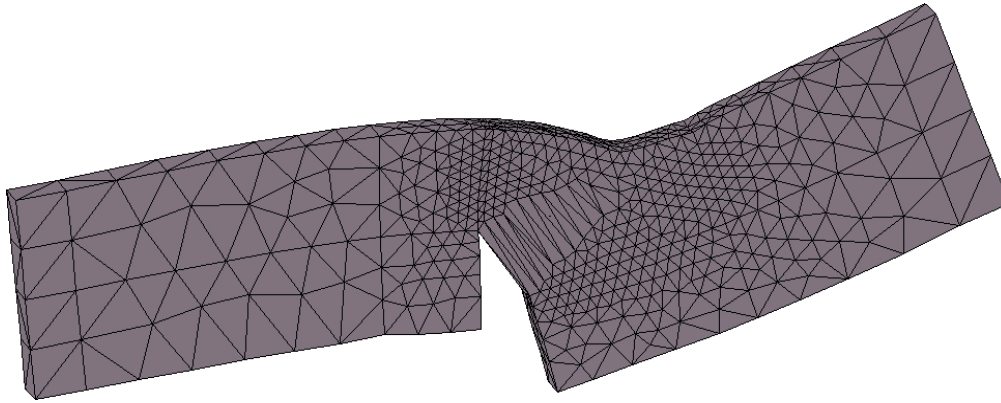
Fig. 9 Crack surface crossing the elements

O.L. Manzoli, G.K.S. Claro, E.A. Rodrigues and J.A. Lopes Jr.

Fig. 10 Deformed mesh after cracking

■ **Domain of the problem**

■ **Limit of the numerical analysis**

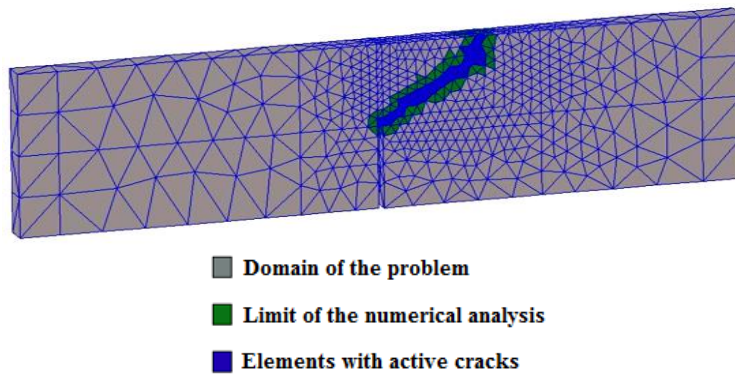■ **Elements with active cracks**

Fig. 11 Domain of the analysis for the proposed algorithm
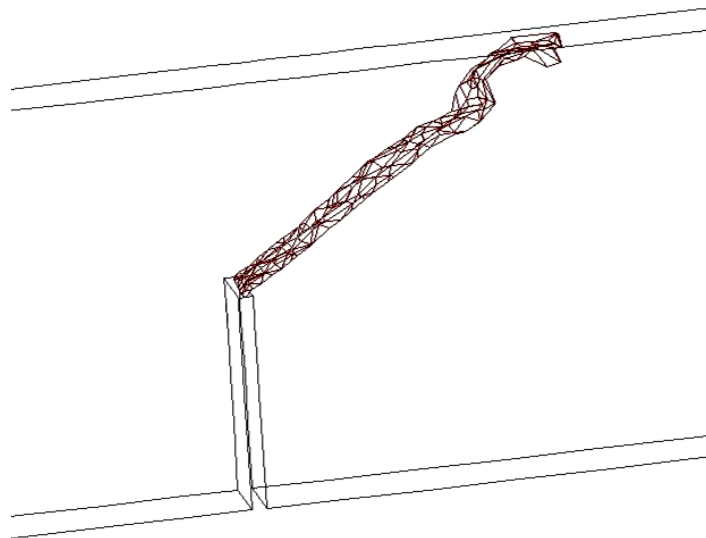
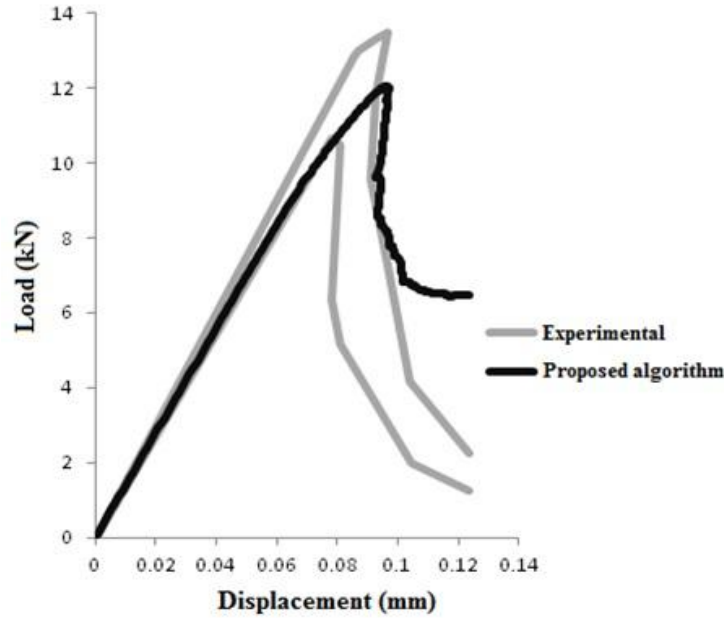

Fig. 12 Crack surface formed at the end of the analysis

Fig. 13 Structural response of the notched beam subjected to four-point bending loads

In this case, the total CPU analysis time was 94.91 seconds (PC Intel® Core™ i5 CPU M460@2.53GHz). The topology process (step 1) took 2.79 seconds (2.9% of the total time) and the local-global tracking scheme was performed 572 times, consuming 6.26 seconds, of which 4.83 seconds were spent to solve the linear systems of equations. Therefore, the total process time spent by the proposed algorithm to generate the mesh topology (step 1), to identify the elements of the crack path and its neighboring elements, to locally renumber the involved elements, nodes and connectivities, to assemble the local stiffness matrices K and to construct the crack surfaces for all iterations was less then 1.43 seconds, corresponding to 1.5% of the total analysis time. This shows that the time consumed for the tasks inherent to the local-global scheme is very short (less than 4.4% of the total time). This short additional time spent by the local-global scheme (the global scheme does not need to perform most of these tasks) is largely compensated by the reduced number of degrees of freedom involved.

Fig. 12 shows the failure surface at the end of the simulation. In this Fig. 12, note the irregularity when the discontinuity is close to the limit of the upper boundary of the material. This irregularity is due to the very complex stress state of this region, without predominance of the normal tensile component.

Fig. 13 shows the comparison between the structural responses obtained experimentally and numerically with the proposed formulation.

5.2 Rectangular block subjected to tensile loading

The second analysis presented here is based on the one presented by Jäger, Steinmann and Kuhl (2008). This analysis involved a rectangular block subjected to tensile loading, with a cross section of 1 mm^2 and height of 2 mm. The block is fixed at the bottom and subjected to a load

distributed over its upper right side (see Fig. 14). The crack starts on the side adjacent to the application of the load, leading to a curved rupture surface.

Fig. 14 presents the mesh of elements used in the numerical analysis, composed of 1025 elements. It should be noted that symmetry was also used in this analysis, simulating half the thickness of the rectangular block. The element indicated as the first one to fail is indicated in red. The assumed parameters of the material were: $G_F = 100$ N/m, $f_t = 2$ N/mm^2, $E = 1000$ MPa and $\nu = 0.2$

Fig. 15 shows the progressive construction of the discontinuity surface in the successive loading steps. The first image represents the loading step in which the first element met the failure criterion, while the last image illustrates the final step of the crack's path, leading to the failure of the block. The failure mechanism is similar to the one obtained.by Jäger *et al.*(2008).
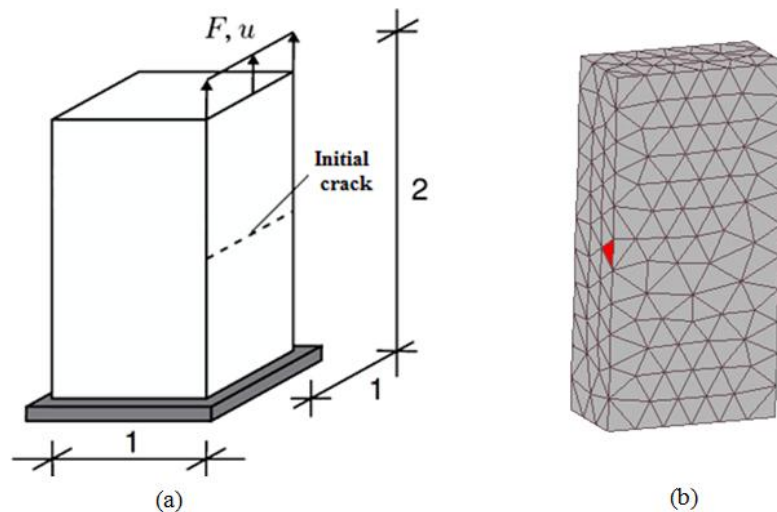
Fig. 14 S Rectangular block subjected to tensile loading. (a) Geometry (in mm) and boundary conditions Jäger *et al.* (2008), (b) finite element mesh
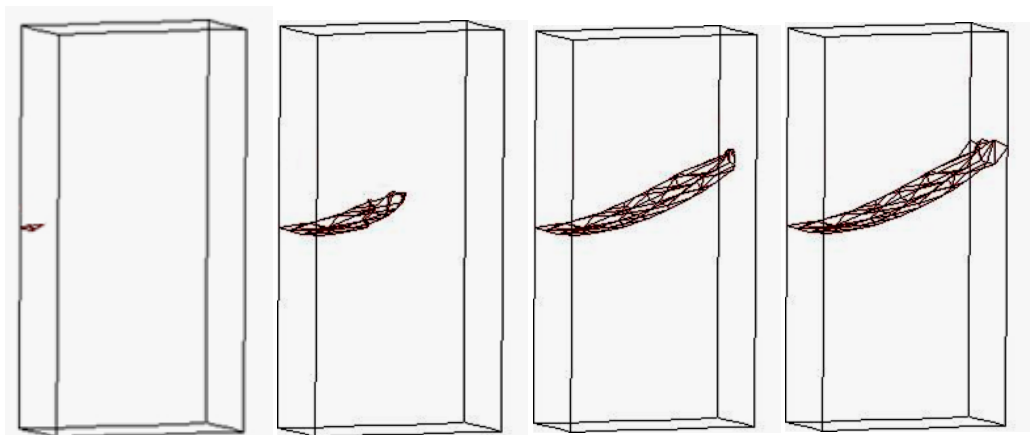
Fig. 15 Progression of the construction of the discontinuity surface on the rectangular block
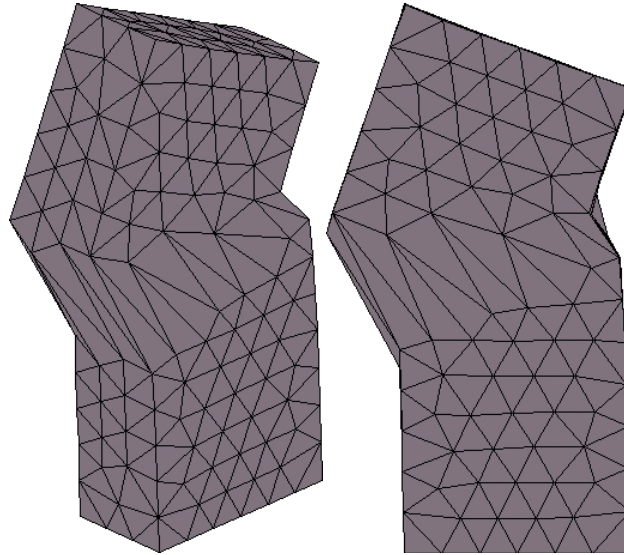
Fig. 16 Deformed mesh at the end of analysis

■ Domain of the problem

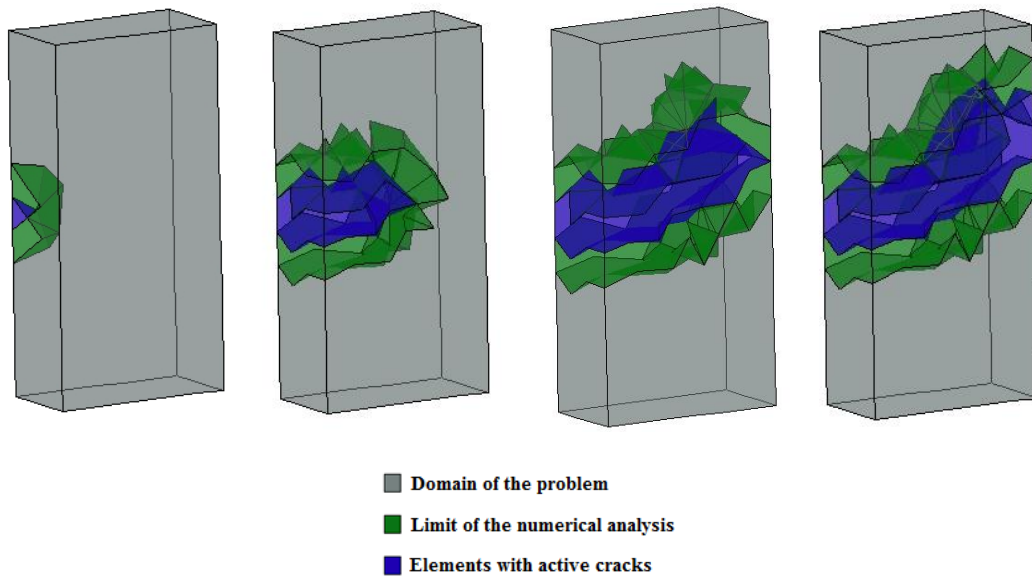■ Limit of the numerical analysis

■ Elements with active cracks

Fig. 17 Evolution of the region of analysis during loading of the rectangular block

Fig. 16 illustrates the deformed mesh in the last stage of the numerical analysis. The failure mechanism obtained by Jäger *et al.* (2008) is similar to the one obtained with the proposed methodology.

The sequence of images in Fig. 17 represents the region affected by the algorithm during the construction of the crack path, where the green color represents the algorithm's analytical limit and

the blue color represents the region composed of the elements that reached active failure. Fig. 18 shows the structural response.

5.3 Brazilian test

The Brazilian fracture test, also analyzed by Chaves (2003), consists of a cylinder compressed along its entire length, keeping the rotation axis parallel to the supports that transmit the compressive load. Fig. 13 shows a concrete cylinder with length $B = 300$ mm and diameter $D = 150$ mm, subjected to a diametral compression P. The properties of the material are: $G_F = 115$ N/m, $f_t = 3.2$ MPa, $E = 32.4$ GPa and $v = 0.2$.

In this case the entire cylinder was simulated using a coarse mesh of 747 finite elements. The failure surface is illustrated in Fig. 20

Fig. 21 illustrates the deformed mesh after the formation of the crack.

In this case, the domain of the analysis of the proposed algorithm represent almost the entire domain of the cylinder, as illustrated in Fig. 22, where the gray elements are the ones not included in the analysis.

Fig. 23 shows the evolution of the applied force vs crack opening at the center of the frontal face of the cylinder.
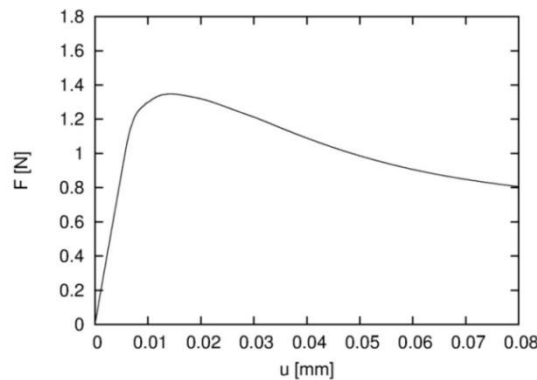

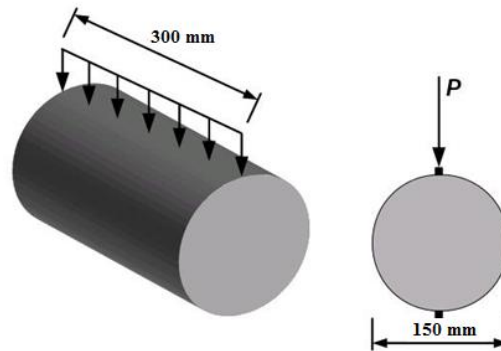Fig. 18 Force vs displacement curve of the rectangular block

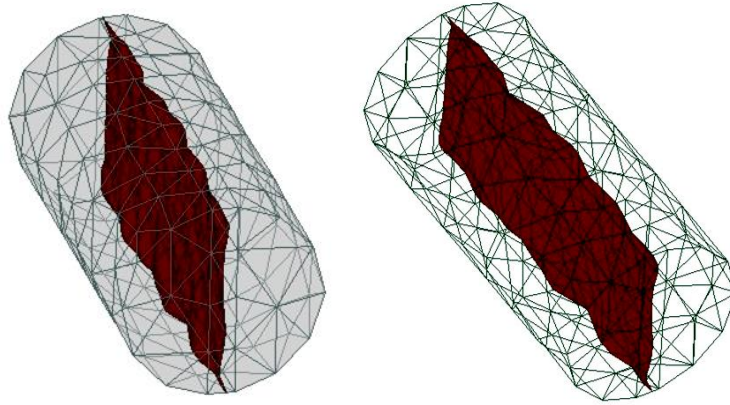Fig. 19 Geometry (in mm) and boundary conditions proposed by Chaves (2003)

Fig. 20 Crack surface formed after the loading process of the Brazilian test, shown from different perspectives
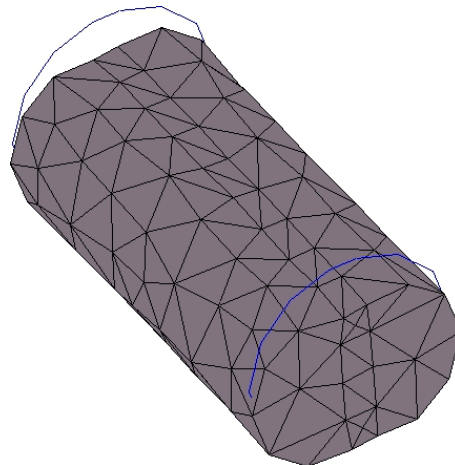

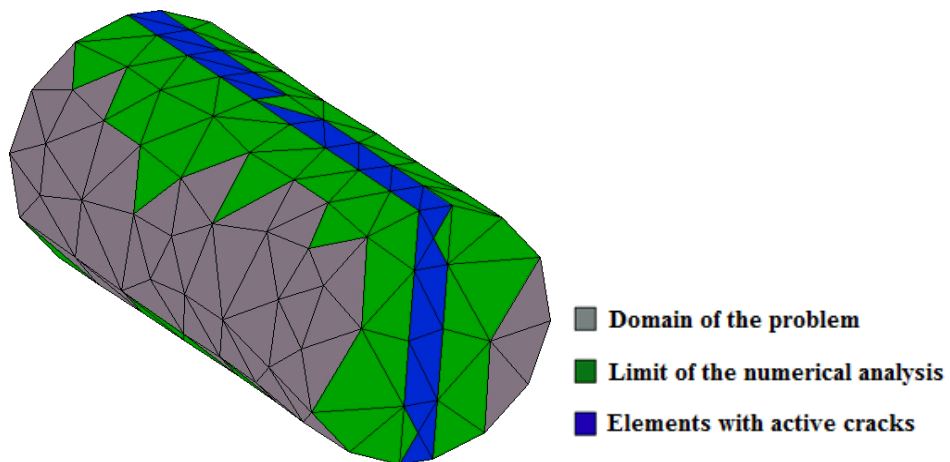Fig. 21 Deformed mesh at the end of the analysis

Fig. 22 Region analyzed by the proposed algorithm in the Brazilian fracture test
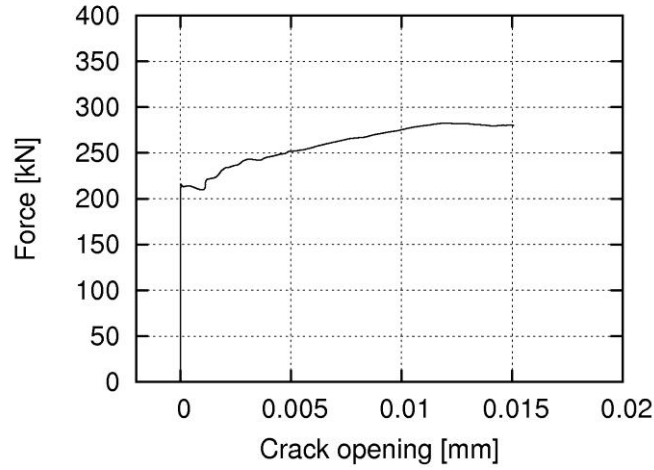
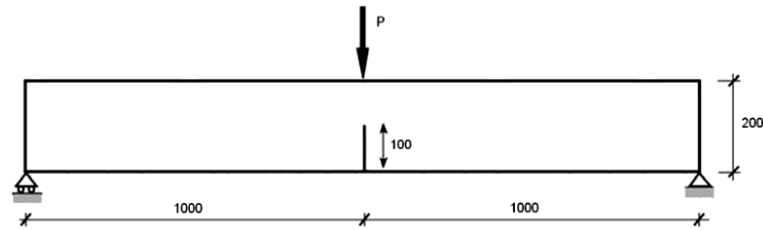Fig. 23 Force vs crack opening curve of the Brazilian Test

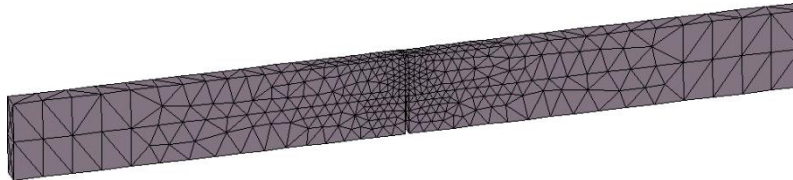Fig. 24 Geometry (in mm) and boundary conditions of the notched concrete beam tested by Petersson (1981)

Fig. 25 Finite element grid used in the analysis of the notched beam subjected to three-point loading

5.4 Notched beam subjected to three-point loading

The last analysis corresponds to an experimental test, presented by Petersson (1981), of a 50-mm-thick notched concrete beam subjected to three-point loading, whose dimensions and geometry are illustrated in Fig. 24.

The properties of the concrete are: $G_F = 124$ N/m, $f_t = 3.33$ MPa, $E = 30.0$ GPa, $v = 0.2$.

In this case, half the thickness of the beam was simulated, using symmetry. The finite element grid used in the numerical analysis is shown in Fig. 25 and is composed of 2262 elements.

In order to demonstrate that the proposed crack tracking algorithm is able to describe the path of the discontinuity in a given vector field of directions normal to the failure surface, a vector field n oriented horizontally, i.e. containing only the component n_1, was used in the simulation.
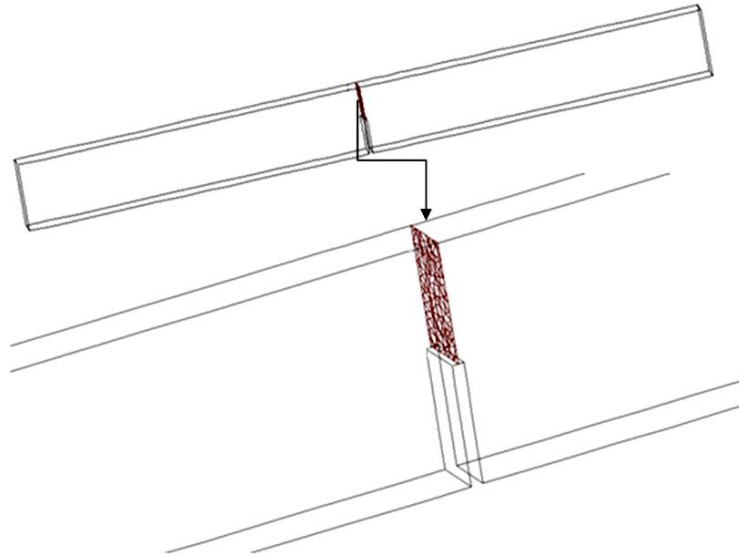
Fig. 26 Crack surface described by the proposed algorithm
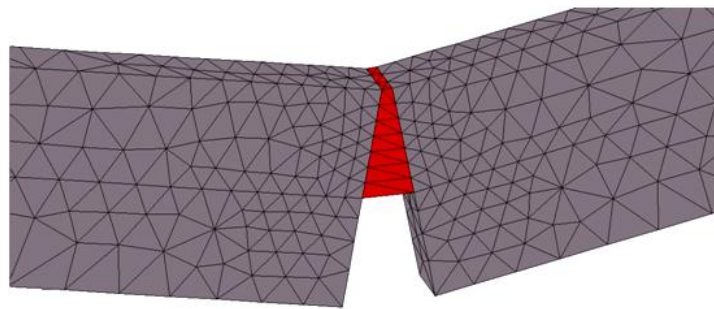

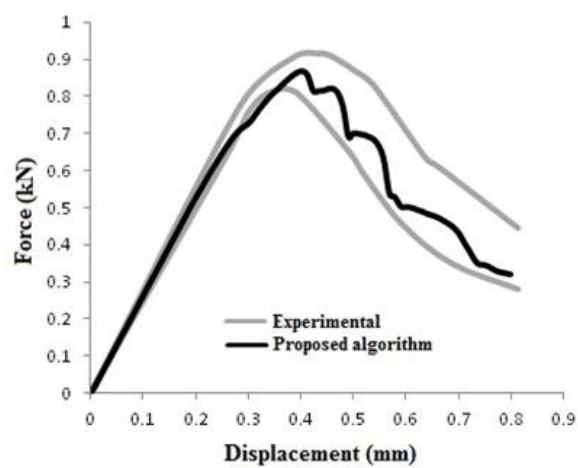Fig. 27 Strain of the tensioned beam, shown from different angles

Fig. 28 Force vs displacement curve of the tensioned beam

As expected, the resulting discontinuity surface is perpendicular to the direction of crack propagation, as shown in Fig. 26.

The surface discontinuity found generated strain in the material, as illustrated in Fig. 27. In this case, this strain acts like a contact surface (adherence) between the parts displaced due to the presence of the crack.

The curve resulting from the analysis was compared with the curve obtained experimentally. In Fig. 28, the gray lines represent the upper and lower limits of the experimental curves, while the black curve represents the simulated result obtained by the proposed algorithm.

6. Conclusions

This paper proposed a crack path tracking algorithm based on the global crack tracking algorithm proposed by Oliver and Huespe (2004), which can minimize the processing time of numerical analyses. An evaluation of the results indicated that, in all the analyses, the proposed algorithm was able to track the crack path using a reduced domain of finite elements in each step of the solution. In contrast, the global algorithm would use all the elements of the mesh in each step of the solution of the numerical analysis.

In the analysis of the notched beam subjected to four-point loading using the proposed algorithm, the final portion of the surface discontinuity presented an irregularity. This was attributed to the fact that the crack surface was established by a criterion based on the maximum principal tensile stress, which may not be well defined in initially compressed regions, as is the case of the region in question. The irregularity at the potential failure surface led to a difference in structural response, which became evident when the force vs. displacement curve found by the proposed algorithm was compared with the experimental curves.

In the analysis of the notched beam subjected to three-point loading, an oriented vector field *n* was used in order to highlight the fact that the proposed algorithm is able to describe the path of the discontinuity, regardless of whether or not this vector field of normal directions of crack propagation corresponds to a stress field.

References

Areias, P.M.A. and Belystschko, T. (2001), "Analysis of three-dimensional crack initiation and propagation using the extended finite element method", *Int. J. Numer. Meth. Eng.*, **50**(4), 993-1013.

Blanco, S. (2007), "Contribuciones a la simulación numérica del fallo material en medios tridimensionales mediante la metodología de discontinuidades fuertes de continuo", Ph.D. Thesis, Universidad Politécnica de Cataluña, Barcelona, Spain.

Chaves, E.W.V. (2003), "A three dimensional setting for strong discontinuities modeling in failure mechanics", Ph.D. Thesis, Universidad Politécnica de Cataluña, Barcelona, Spain.

Galvez, J.C., Elices, M., Guinea, G.V. and Planas, J. (1998), "Mixed mode fracture of concrete under proportional and non-proportion al loading", *Int. J. Fract.*, **94**, 267-284.

Gasser, T.C. and Holzapfel, G.A. (2006), "3D Crack propagation in unreinforced concrete. A two-step algorithm for tracking 3D crack paths", *Comput. Meth. Appl. Mech. Eng.*, **195**, 5198-5219.

Hughes, T.J.R. (2000), *The Finite Element Method – Linear Static and Dynamic Finite Element Analysis*, Ed. Dover, United States of America – Mineola.

Jäger, P., Steinmann, P. and Kuhl, E. (2008), "Modeling three-dimensional crack propagation – A

comparison of crack path tracking strategies", *Int. J. Numer. Meth. Eng.*, **76**, 1328-1352.

Manzoli, O.L. (1998), "Un modelo analítico y numérico para La simulación de discontinuidades fuertes em La mecánica de sólidos", Doctoral Thesis, Universidad Politécnica de Cataluña, Barcelona, Spain.

Manzoli, O.L. and SHING, P.B. (2006), "A general technique to embed non-uniform discontinuities into standard solid finite elements", *Comput. Struct.*, **84**, 742-757.

Manzoli, O.L. (2008), *Contribuições à simulação numérica de descontinuidades fortes*, Tese (Livre Docência) – Universidade Estadual Paulista "Júlio de Mesquita Filho" – Faculdade de Engenharia de Bauru, Bauru, São Paulo.

Manzoli, O.L., Rodrigues, E.A., Claro, G.K.S. and Motta, C.E.Q. (2010), "Simulação do comportamento não linear de materiais quase-frágeis via elementos finitos com fissura embebida", *Asociación Argentina de Mecánica Computacional*, **19**, 5341-5356.

Melenk, J.M. and Babuska, I. (1996), "Partition of unity finite element method: basic theory and applications", *Comput. Meth. Appl. Mech. Eng.*, **139**, 289-314.

Oliver, J. and Huespe, A.E. (2004), "Continuum approach to material failure in strong discontinuity settings", *Comput. Meth. Appl. Mech. Eng.*, **193**, 3195-3220.

Oliver, J., Huespe, A.E. and SÁNCHEZ, P.J. (2006), "A comparative study on finite elements for capturing strong discontinuities", E-FEM vs X-FEM, *Comput. Meth. Appl. Mech. Eng.*, **195**, 4732-4752.

Oliver, J., Linero, D.L., Huespe, A.E. and ManZori, O.L. (2008), "Two-dimensional modeling of material failure in reinforced concrete by means of a continuum strong discontinuity approach", *Comput. Meth. Appl. Mech. Eng.*, **197**, 332-348.

Ortiz, M., Leroy, Y. and Needleman, A. (1987), "A finite element method for localized failure analysis", *Comput. Meth. Appl. Mech. Eng.*, **61**, 189-214.

Peterson, P.E. (1981), Crack Growth and Development of Fractures Zones in Plain Concrete and Similar Materials, Report n TVBM-1006, Div. Build. Mater., Lund Institute of Technology, Lund, Sweden.

CC